Journal of
Ceramic Science
and Technology

J. Ceram. Sci. Tech., **05** [03] 173-183 (2014)
DOI: 10.4416/JCST2014-00003
available online at: http://www.ceramic-science.com

Solid Solution in $LnTiO_2N$ and $MTaO_2N$ Oxynitrides, Ln = La,Nd; M = Ca, Sr, Ba

J. Ahchawarattaworn and D.P. Thompson*

School of Chemical Engineering and Advanced Materials, University of Newcastle, Newcastle upon Tyne, NE1 7RU, U.K.

received February 12, 2014; received in revised form April 04, 2014; accepted May 09, 2014

Abstract

The last fifty years have witnessed a considerable level of interest in the field of oxynitrides. This has mainly been because of their thermal and mechanical properties, but certain members of this group have the perovskite atomic arrangement, and as such might be expected to have interesting electrical and electronic properties. Foremost among these are the rare earth titanium oxynitrides, $LnTiO_2N$, with Ln = La and Nd the two rare earths most commonly investigated, and also the Group II tantalum oxynitrides of the type $MTaO_2N$ where M = Ca, Sr and Ba. The present paper explores the changes in structure which occur in solid solutions between end-members of these two series. In the $(La_pNd_{1-p})O_2N$ series, the Pnma space group of the Nd end-member is retained up to p = 0.8 in the above formula; in the $(Ba_pSr_{1-p})TaO_2N$ series, the cubic structure of $BaTaO_2N$ is retained up to p ~ 0.5 before transforming into the tetragonal modification of $SrTaO_2N$; in the $(Ca_pSr_{1-p})TaO_2N$ series, the tetragonal structure of $SrTaO_2N$ is stable up to p ~ 0.65 before changing into the orthorhombic form of $CaTaO_2N$. No evidence was found for solid solutions between $CaTaO_2N$ and $BaTaO_2N$.

Keywords: Oxynitrides, perovskites, synthesis, crystal structure, dielectric properties

I. Introduction

Cubic and lower symmetry perovskites provide some of the most important electroceramic materials currently in use because of their wide diversity of electrical and electronic properties. The vast majority are oxides, with a wide spectrum of metallic elements occupying the A and B sites in the ABO_3 general formula. Non-oxide perovskites have received much less attention, but in view of the impressive success of their oxide counterparts, these have attracted the interest of researchers, particularly with a view to exploring their dielectric properties. Oxynitrides [1] have been a significant area of research for the last 50 years, generally because of their good thermal and mechanical properties, but various members of this group exhibit perovskite structures and are therefore of interest for electrical/electronic property exploration. The simplest perovskite oxynitrides are of the type ABO_2N; compared with oxides, the substitution of one nitrogen for one oxygen atom requires the introduction of a higher valent metal cation in either the A or B sites. For a tetravalent B cation, the A cation must be trivalent, and combined with the additional requirement that the A site is large, the most attractive candidates are rare earth cations. In the case of a pentavalent B cation, the A site must be occupied by a divalent cation, and again bearing in mind size requirements, the Group II elements of calcium, strontium and barium are the obvious contenders.

* Corresponding author: derek.thompson@ncl.ac.uk

Marchand *et al.* [2] synthesised $BaTaO_2N$, $BaNbO_2N$, $SrTaO_2N$ and $CaTaO_2N$ (hereafter referred to as $MTaO_2N$ oxynitrides) and considered them to be potential high dielectric constant dielectric materials. However, Gouin *et al.* [3] claimed that by comparison with the infrared spectrum of $BaTiO_3$, $BaTaO_2N$ did not show a soft polar mode, so the dielectric response should not reach as high a value. Later work by Kim *et al.* [4], using powder samples compacted by means of cold isostatic pressing to 55 % of theoretical density, found high dielectric constants of 2900 and 4900 for $SrTaO_2N$ and $BaTaO_2N$ respectively at room temperature. In contrast, $CaTaO_2N$ was found to have a much lower dielectric constant (k~30). These researchers also observed metallic conductivity for $BaNbO_2N$, which most likely resulted from partial reduction of niobium from oxidation state +5 to +3, thereby leading to the introduction of charge carriers in the conduction band.

Lanthanide-based perovskite oxynitrides of the type $LnTiO_2N$ were first synthesised by means of ammonolysis of the appropriate mixed ternary oxide powders at a temperature of 950 °C by Marchand *et al.* [5] and then by Clarke *et al.* [6]. Repeated ammonolysis with intermediate regrinding was needed to produce a pure product. No dielectric data were reported for these compounds.

The present study arose as a result of considering the deviations from cubic symmetry exhibited by these two groups of oxynitrides, about which there is some unclarity in the literature. It would appear that in the $MTaO_2N$

series, $BaTaO_2N$ is cubic [7], whereas $SrTaO_2N$ is tetragonal and $CaTaO_2N$ is orthorhombic (Günther *et al.* [8]) this type of symmetry degeneration is not uncommon in perovskites as the size of the A cation decreases. $LaTiO_2N$ was originally thought to have a simple perovskite cell [2,5] but subsequent more precise work based on neutron diffraction (Clarke *et al.* [6]) reported it as being of lower symmetry, and their Rietveld refinements only converged satisfactorily if a triclinic unit cell was adopted. However, the departure from orthogonality is very small (α = 90.199°, β = 90.154°, γ =89.988°), and more recent work by Yashima *et al.* [9] based on electron diffraction argued that the structure was orthorhombic with the relatively rare Imma space group. Clarke *et al.*'s [6] neutron diffraction data for $NdTiO_2N$ did refine satisfactorily assuming the more common $GdFeO_3$-type Pnma orthorhombic perovskite arrangement. Both the Imma $LaTiO_2N$ and the Pnma $NdTiO_2N$ unit cells have similar dimensions (a_o, b_o, c_o) related to the basic cubic perovskite unit cell edge-length, a_p, by the relationships $a_o = \sqrt{2}a_p$, $b_o = 2a_p$, $c_o = \sqrt{2}a_p$. Whichever space group is correct for $LaTiO_2N$, it is clear that at some point between $LaTiO_2N$ and $NdTiO_2N$ there is a change in space group, and because the most interesting electrical properties occur close to compositions where there are structural transformations, an important aim of the present paper was to identify at what composition this transformation occurred in the (La,Nd)TiO_2N system.

Pors *et al.* [7] studied $Ba_pSr_{1-p}TaO_2N$ solid solutions, and found that the cubic structure of $BaTaO_2N$ was retained up to p=0.56, before transforming into the tetragonal $SrTaO_2N$ form. As far as the present authors are aware, no data have been published on mixed barium/calcium, strontium/calcium or barium/calcium $MTaO_2N$ oxynitrides. The present work therefore also included a study of solid solutions series between pairs of these oxynitrides, with the aim of identifying compositions at which symmetry changes occurred.

II. Experimental

All samples were prepared by the action of fast-flowing ammonia on appropriate mixtures of oxides at 900 – 1000 °C. $MTaO_2N$ derivatives were prepared from mixtures of Ta_2O_5 (Sigma-Aldrich, 99 %; loss on ignition 0.5 %; metal oxide impurities all < 0.005 %) plus the carbonates $BaCO_3$, (Merck BDH Analar 99 %), $SrCO_3$, (Sigma-Aldrich 99 %), $CaCO_3$, Sigma-Aldrich 99 %), all with alkaline earth carbonates < 0.7 % as major impurities. $LnTiO_2N$ products were prepared from mixtures of TiO_2 (Merck (BDH Analar) 99 %, loss on ignition 0.5 %, metal oxide impurities all < 0.005 %) plus either La_2O_3 (Sigma-Aldrich 99.9 %), Nd_2O_3 (Sigma-Aldrich 99.9 %) or mixtures, both with < 0.1 % of mainly rare earth oxide impurities. All powders were of particle size less than 5 μm.

Small quantities of the appropriate chemical powders (~ 5 g) were thoroughly hand mixed in an agate pestle and mortar in isopropanol. The slurry was stirred under an infra-red lamp for 15 – 20 minutes to evaporate the isopropanol depending on the particle size. The most commonly used technique of ball-milling was avoided because of contamination from the inevitably abraded milling media. In some cases, the mixed powders were compacted into pellets and then pre-reacted in air to form ternary oxide precursors; in other cases the binary powders were directly heated in flowing ammonia gas. La_2O_3 is extremely sensitive to moisture present in the air which hydrolyses it to $La(OH)_3$; this powder was therefore pre-dried at 900 °C for 16 hours before use as a starting material.

Effective nitridation by ammonolysis depends critically on the diffusion of atomic nitrogen into oxide grains, and loose powders were therefore used to facilitate gas access. Approximately 3 g of starting powder was heated at a rate of 10 °C/min to the target temperature and held at that temperature for 16 hours prior to cooling to room temperature also at a rate of 10 °C/min. After nitriding, powders were re-ground and re-nitrided until a pure product sample had been achieved. Intended chemical reactions for pre-reacted powders were:

$$Ln_2Ti_2O_7 + 2NH_3 \rightarrow 2LnTiO_2N + 3H_2O \quad (1)$$

$$M_2Ta_2O_7 + 2NH_3 \rightarrow 2MTaO_2N + 3H_2O \quad (2)$$

Since the compound $Ba_2Ta_2O_7$ does not exist, mixed binary oxide powders were directly nitrided in ammonia, the intended reaction being:

$$2BaCO_3 + Ta_2O_5 + 2NH_3 \rightarrow 2BaTaO_2N + 3H_2O + 2CO_2 \quad (3)$$

This reaction was also explored for other Group II carbonates to compare the effectiveness with Equations (1) and (2) above. For all reaction routes, mixtures of rare earth oxides (for $LnTiO_2N$ products) and Group II starting compounds (for $MTaO_2N$ products were used.

Product phases were identified by means of x-ray diffraction using a Panalytical X-Pert PRO system and CuKα radiation. Unit cell dimensions and Rietveld refinement were carried out using the Highscore plus software available on the X-Pert PRO system.

III. Results

(1) $LnTiO_2N$ oxynitrides

Preliminary experiments focused on nitriding pre-prepared ternary oxides of general formula $Ln_2Ti_2O_7$. It soon became clear that whereas the nitriding of $La_2Ti_2O_7$ using ammonia proceeded quickly, the rate of nitridation decreased markedly on moving to higher atomic number rare earths. The investigation was therefore restricted to just lanthanum and neodymium. Cerium, intermediate in atomic number between lanthanum and neodymium, was also explored, but the transition between oxidation states (+4 at room temperature; +3 above ~ 1200 °C) resulted in a variety of different phases in the products; this work was therefore not pursued.

$La_2Ti_2O_7$ was prepared by means of solid state reaction of the binary oxides at 1200 °C for 5 hours followed by 1350 °C for a further 16 hours. Nitridation in ammonia for 16 hours at 950 °C followed by re-grinding of the product and a further nitridation under identical conditions gave a pure spectrum of $LaTiO_2N$ as shown in Fig. 1.

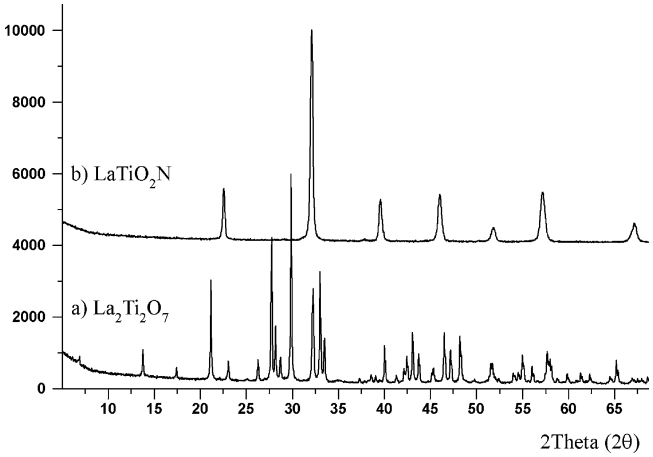

Fig. 1: X-ray diffraction patterns of (a) $La_2Ti_2O_7$, and (b) $LaTiO_2N$.

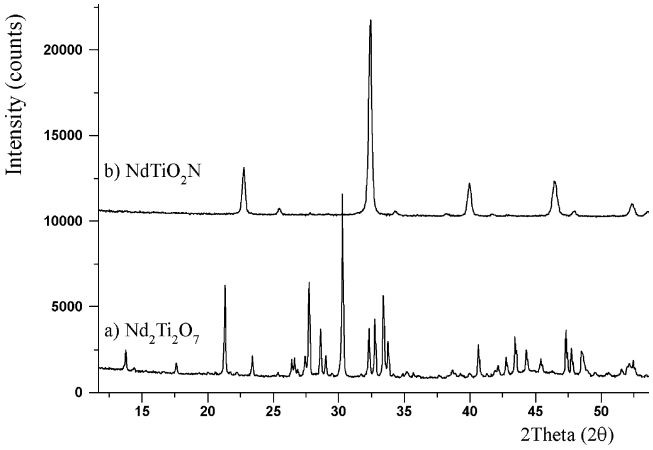

Fig. 2: X-ray diffraction patterns of (a) $Nd_2Ti_2O_7$, and (b) $NdTiO_2N$.

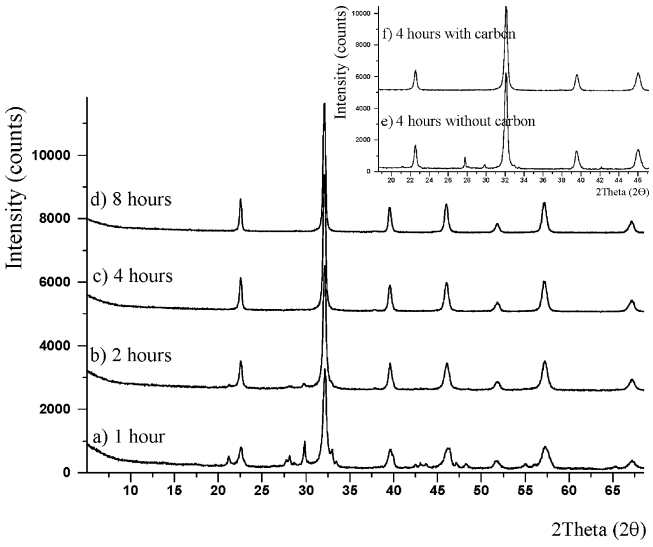

Fig. 3: X-ray diffraction patterns of $LaTiO_2N$ prepared with 1 wt% carbon added.

Nitridation of $Nd_2Ti_2O_7$ under identical conditions gave a > 95 % pure sample of $NdTiO_2N$ (Fig. 2), and a further regrinding plus re-nitridation step was required to eliminate the trace amounts of un-nitrided phases. In an attempt to speed up the nitriding step, small amounts of carbon were included in the starting mix prior to ammonia treatment. Fig. 3 shows the effect of adding 1 wt% of carbon, and it is clear that this is very effective in speeding up the rate of nitridation, with an essentially pure product being achieved after about 3 hours of nitridation. However, since the aim of the present work was ultimately to use the products for dielectric measurements, and even trace amounts of residual carbon would be detrimental, the carbon-free route was used for preparing samples. Single-phase compositions of the type $La_pNd_{1-p}TiO_2N$ (p = 0, 0.2, 0.4,...1.0) were synthesized by ammonolysis of pre-prepared $(La_pNd_{1-p})_2Ti_2O_7$ samples at 950 °C for 16 hours. The ternary oxide precursors were made based on solid-state reaction between the corresponding Ln_2O_3 and TiO_2 powders as described above. The x-ray diffraction traces in Fig. 4 confirm the single-phase nature of the products, and demonstrate a systematic variation in unit cell dimensions across the series (Fig. 5). These powders were then reground and introduced in powder form into the ammonia nitriding furnace. Whereas for La-rich samples just a single regrinding step was needed to achieve single-phase products, for the Nd-rich samples, two re-grinding steps were needed. The colour of the resulting powder ranged from dark greenish brown for $NdTiO_2N$ through to the dark brown of $LaTiO_2N$. Fig. 6 shows x-ray diffraction patterns of the resulting products, showing the existence of a complete range of solid solution across the $La_pNd_{1-p}TiO_2N$ system. It was noted that peak-widths for end-member compositions were less than for intermediate compositions, consistent with the expectation that achieving good quality mixing in a mixed powder preparation route is difficult to achieve, and as a result the final products covered a small range of La:Nd compositions.

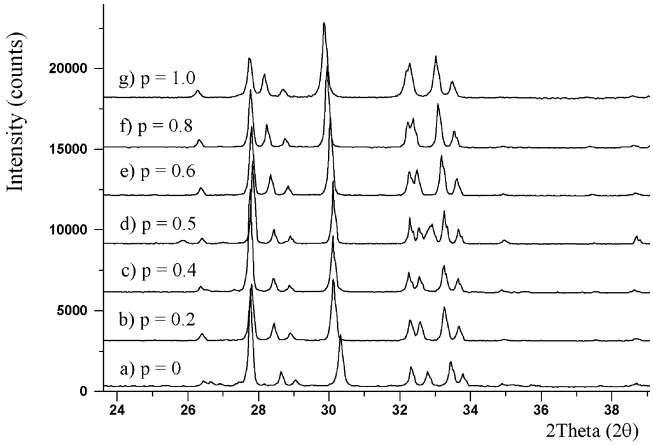

Fig. 4: X-ray diffraction patterns of $(La_pNd_{1-p})_2Ti_2O_7$ solid solutions.

The structures of all compositions were refined by means of Rietveld analysis. For $LaTiO_2N$, the quality of the x-ray powder data was insufficient to unambiguously identify the triclinic cell of Clarke *et al.* [6], and therefore the Imma cell of Yashima *et al.* [9] was used, starting with their refined atomic parameters and isotropic temperature factors (the latter being kept constant throughout the refinement). A disordered distribution of nitrogen and oxygen atoms in non-metal sites was assumed. Table 2 shows that the final parameters from the present refinement of $LaTiO_2N$ were in satisfactory agreement with the values of Yashima

et al. [9] (shown alongside), and the final R_p value of 3.9 was also satisfactory. For $NdTiO_2N$, the refined parameters of Clarke *et al.* [6] were used as starting parameters, again keeping isotropic temperature factors constant and assuming a disordered distribution of oxygen and nitrogen atoms. The final refined atomic parameters are shown in Table 1, with the Clarke *et al.* [6] figures alongside. The agreement is satisfactory, as also is the final R_p value of 4.0.

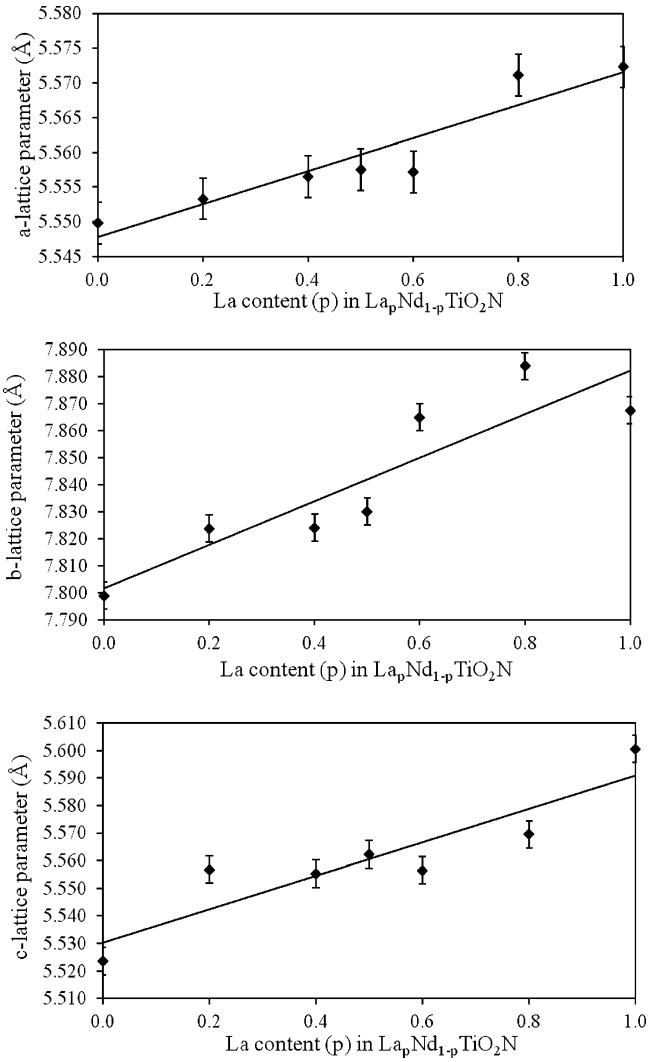

Fig. 5: Unit cell dimensions of $La_pNd_{1-p}TiO_2N$ solid solutions.

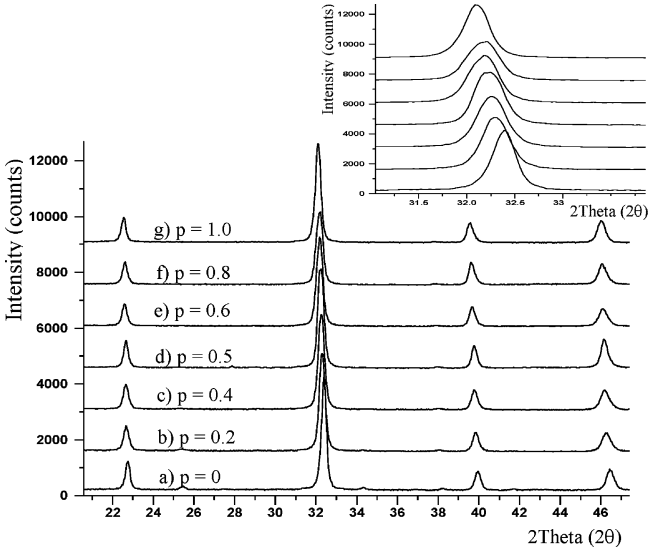

Fig. 6: X-ray diffraction patterns of $La_pNd_{1-p}TiO_2N$ solid solutions.

When the structures of intermediate compositions in the $LdTiO_2N$ – $NdTiO_2N$ series were refined, it was immediately found to be more difficult to get good final R factors. This may partly have been due to the difficulty of getting compositional homogeneity, resulting in some variation in composition in each sample, which made profile fitting more difficult. All compositions were refined in both space groups Imma and Pnma, and it was hoped that there would be a clear indication at some composition that there was a transition between the two space groups. However, R indices were very similar in both space groups throughout the whole series.

Since R-indices alone could not be used to elucidate this information, alternative indicators were sought. The most accurately determined variables in the refinement were the x and z parameters of the La,Nd atoms, and it is clear that these deviated most from x = 0 and z = 0 in $NdTiO_2N$ and gradually converged to zero values when Imma symmetry was achieved. A plot of these coordinates as a function of composition (Fig. 7) shows that the La x coordinate becomes zero at a value close to 0.8, and the z coordinate similarly. Clearly, the Imma space group takes over at compositions close to this point and is then retained up to pure $LaTiO_2N$.

Table 1: Refined atomic coordinates for $La_pNd_{1-p}TiO_2N$ in space group *Pnma* for compositions in the range $0 \le p \le 0.8$.

Atom	Wyckoff	Occupancy	x	y	z	R_p, R_{wp}(%)
p = 0						3.95, 4.11
Nd	4c	1	0.0298(3)/0.03175	¼	0.9919(7)/0.9955	
Ti	4b	1	½	0	0	
O/N(1)	4c	0.67/0.33	0.491(3)/0.4853	¼	0.073(6)/0.0755	
O/N(2)	8d	0.67/0.33	0.309(3)/0.2850	0.030(3)/0.03934	0.736(4)/0.7161	
p = 0.2						4.43, 5.75
La/Nd	4c	0.2/0.8	0.0175(4)	¼	0.9950(5)	

Continuing Table 1

Atom	Wyckoff	Occupancy	x	y	z	R_p, R_{wp}(%)
Ti	4b	1	½	0	0	
O/N(1)	4c	0.67/0.33	0.523(4)	¼	0.078(3)	
O/N(2)	8d	0.67/0.33	0.214(8)	0.014(5)	0.720(4)	
p = 0.4						4.54, 5.87
La/Nd	4c	0.4/0.6	0.0182(4)	¼	0.9972(7)	
Ti	4b	1	½	0	0	
O/N(1)	4c	0.67/0.33	0.533(4)	¼	0.085(3)	
O/N(2)	8d	0.67/0.33	0.224(9)	0.007(4)	0.727(6)	
p = 0.5						4.53, 5.86
La/Nd	4c	0.5/0.5	0.0163(4)	¼	0.9931(5)	
Ti	4b	1	½	0	0	
O/N(1)	4c	0.67/0.33	0.524(5)	¼	0.057(5)	
O/N(2)	8d	0.67/0.33	0.210(9)	0.012(4)	0.727(7)	
p = 0.6						4.86, 6.33
La/Nd	4c	0.6/0.4	0.0130(6)	¼	0.9988(8)	
Ti	4b	1	½	0	0	
O/N(1)	4c	0.67/0.33	0.520(6)	¼	0.060(6)	
O/N(2)	8d	0.67/0.33	0.23(1)	0.036(4)	0.740(7)	
p = 0.8						6.36, 8.09
La/Nd	4c	0.8/0.2	0.006(1)	¼	0.001(1)	
Ti	4b	1	½	0	0	
O/N(1)	4c	0.67/0.33	0.54(1)	¼	0.032(6)	
O/N(2)	8d	0.67/0.33	0.238(7)	0.44(3)	0.726(6)	

Table 2: Refined atomic coordinates for $La_pNd_{1-p}TiO_2N$ in space group *Imma* for $0.8 \leq p \leq 1.0$.

	Wyckoff	Occupancy	x	y	z	R_p, R_{wp}
p=0.8						6.14, 7.88
La/Nd	4e	0.8/0.2	0	¼	0.9962(8)	
Ti	4b	1	0	0	½	
O/N(1)	4e	0.67/0.33	0	¼	0.505(9)	
O/N(2)	8 g	0.67/0.33	¼	0.045(2)	¼	
p=1.0						3.86, 5.12
La	4e	1	0	¼	0.001(1)/0.998	
Ti	4b	1	0	0	½	
O/N(1)	4e	0.67/0.33	0	¼	0.581(3)/0.562	
O/N(2)	8 g	0.67/0.33	¼	0.018(3)/0.032	¼	

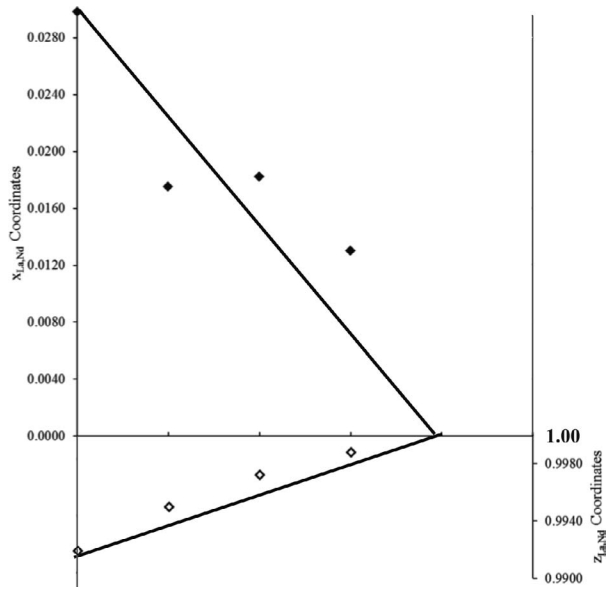

Fig. 7: Variation in x and z coordinates of the La,Nd atom with composition across the $La_pNd_{1-p}TiO_2N$ series.

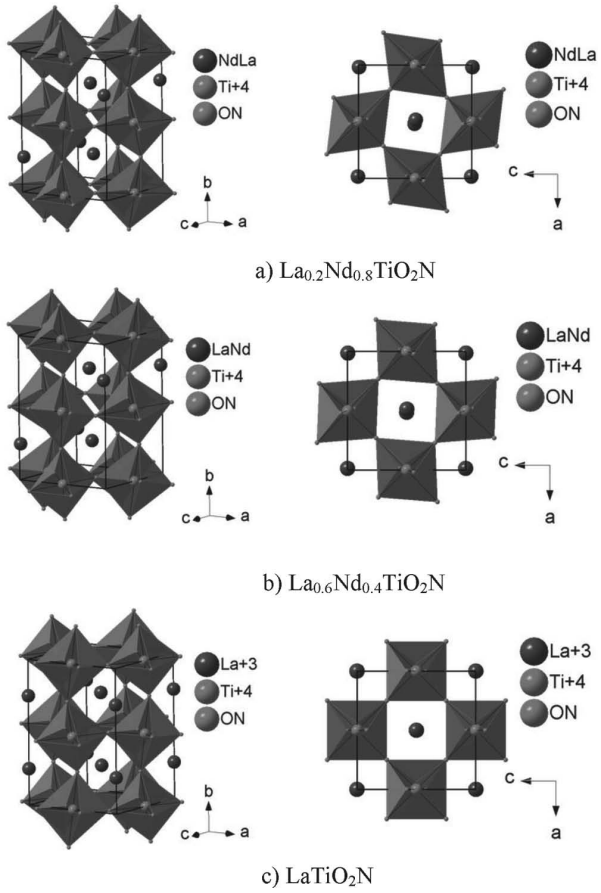

Fig. 8: [001] and [010] projections of the (a) p= 0.2, (b) p = 0.6, and (c) p = 1.0 compositions showing the gradual change in tilt of octahedra as a function of p.

Another useful indicator is the deviation of the octahedra from their "perfect" aligned positions in a cubic perovskite. Fig. 8 shows [001] and [010] projections of the p = 0.2, 0.6 and 1.0 compositions, the latter showing only one layer of octahedra. It is clear from the [010] projections that with increasing p value, the departure of the octahedra from perfect orthogonality decreases, giving the additional mirror plane of symmetry required by the Imma space group at approximately p = 0.8. Refinement of the p = 0.8 composition in both space groups resulted in equally good refinements, Imma giving slightly lower R indices, but the accuracy of the data was not sufficient to allow a unique discrimination between the two possibilities. In summary therefore, it was concluded that Pnma symmetry is retained throughout most of the solid solution series between $NdTiO_2N$ and $LaTiO_2N$, with the transition to Imma occurring at the lanthanum-rich end close to p = 0.8 in the general formula $La_pNd_{1-p}TiO_2N$.

(2) Alkaline earth tantalum oxynitrides

(a) *The (Ba,Sr)TaO_2N series.*

$Ba_pSr_{1-p}TaO_2N$ solid solutions were previously reported by Pors *et al.* [7], who found that when synthesised by means of ammonolyis at 950 °C for 15 hours, a cubic solid solution range extended up to p = 0.56 with the same structure as the cubic end-member, $BaTaO_2N$. In the present work, the range of composition was extended up to the strontium end-member to determine whether other structural changes occurred between the p = 0.56 composition and the tetragonal $SrTaO_2N$. As with the work of Pors *et al.* [7], samples were prepared by direct ammonia nitridation of oxide and carbonate mixed powders, x-ray diffraction spectra of the resulting oxynitrides being shown in Fig. 9.

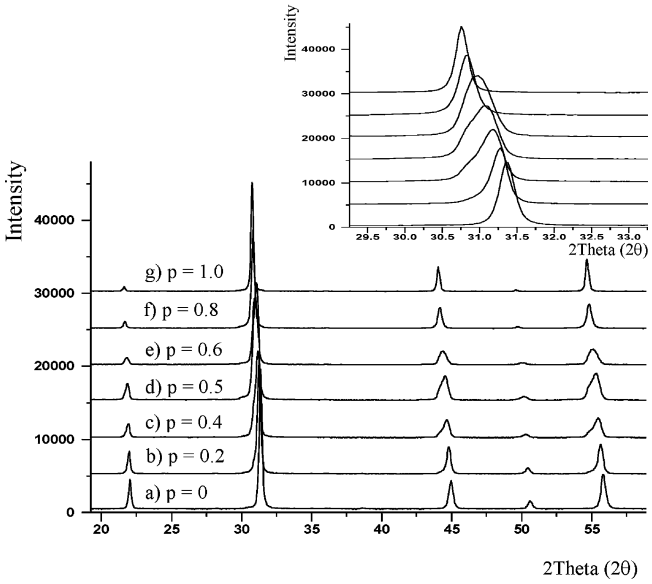

Fig. 9: X-ray diffraction patterns of $Ba_pSr_{1-p}TaO_2N$ solid solutions.

Visual inspection of the patterns showed very little peak asymmetry at the ends of the range, but very clear distortion for the 0.2 < p < 0.6 compositions. Attempts to fit a simple cubic cell to the complete range gave lattice parameters which clearly showed a break in slope at about the p = 0.56 composition as concluded by Pors *et al.* [7] (Fig. 10). However, refinement of the data on a tetragonal structure model (Fig. 11) with unit cell dimensions of a ~ 5.7Å, c ~ 8.1 Å showed a similar break in slope close to the p = 0.6 point especially for the a parameter. Rietveld refinements (Table 3) of the structures on the basis of tetragonal for

$0 < p < 0.5$ and simple cubic for $0.8 < p < 1.0$ all gave excellent refinements with R_p values less than 4 %, whereas the $p = 0.6$ and $p = 0.7$ compositions gave higher R indices, probably because there was a range of compositions present in each sample, resulting in a mix of cubic and tetragonal modifications coexisting.

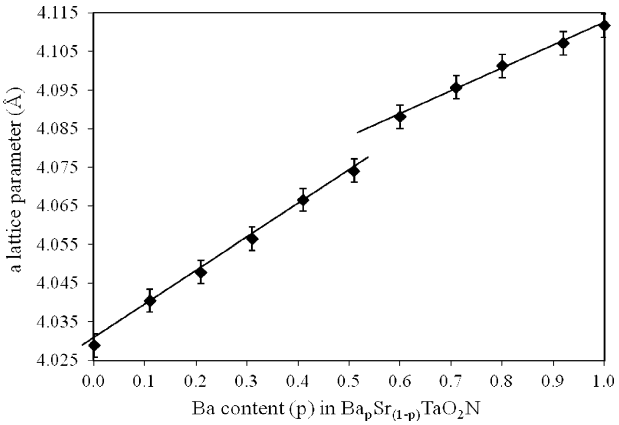

Fig. 10 : Variation in lattice parameter of $Ba_pSr_{1-p}TaO_2N$ versus Ba content on the assumption of a simple cubic structure model.

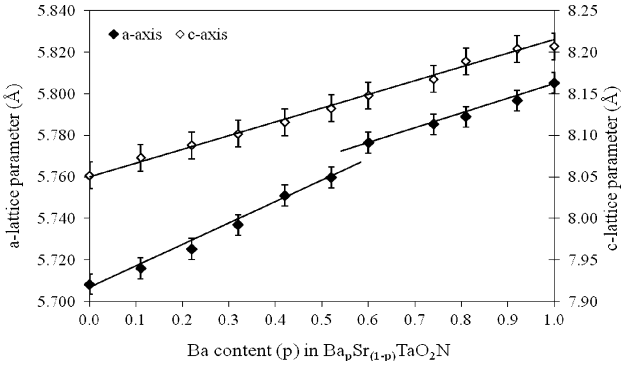

Fig. 11 : Variation in unit cell dimensions of $Ba_pSr_{1-p}TaO_2N$ versus Ba content on the assumption of a tetragonal structure model.

In Table 3, there is a very slight systematic increase in y and z coordinates for the O/N(2) atom, but this is barely more than the standard deviation. It is perhaps surprising that larger displacement towards the cubic values (0.75 and 0.25 respectively) were not observed. Otherwise, the results were entirely in agreement with expectations for this series.

Table 3: Refined atomic coordinates for tetragonal I4/mcm $Ba_pSr_{1-p}TaO_2N$.

Atom	Wyckoff	Occupancy	x	y	z	R_p, R_{wp}
p = 0						2.43, 3.18
Sr	4b	1.000(7)	0	½	¼	
Ta	4c	1.0	0	0	0	
O/N(1)	4a	1.0	0	0	¼	
O/N(2)	8h	1.0	0.769(2)	0.269(2)	0	
p = 0.2						2.11, 3.11
Ba/Sr	4b	0.22(3)/0.78(3)	0	½	¼	
Ta	4c	1.0	0	0	0	
O/N(1)	4a	1.0	0	0	¼	
O/N(2)	8h	1.0	0.771(5)	0.271(5)	0	
p = 0.4						2.28, 3.48
Ba/Sr	4b	0.42(3)/0.58(3)	0	½	¼	
Ta	4c	1.0	0	0	0	
O/N(1)	4a	1.0	0	0		
O/N(2)	8h	1.0	0.774(5)	0.274(5)	0	
p = 0.5						2.34,3.60
Ba/Sr	4b	0.52(2)/0.48(2)	0	½	¼	
Ta	4c	1.0	0	0	0	
O/N(1)	4a	1.0	0	0	¼	
O/N(2)	8h	1.0	0.776(2)	0.276(2)	0	
p = 0.6						2.42, 3.76
Ba/Sr	4b	0.60(4)/0.40(4)	0	½	¼	
Ta	4c	1.0	0	0	0	
O/N(1)	4a	1.0	0	0	¼	
O/N(2)	8h	1.0	0.778(4)	0.278(4)	0	

(b) ***The (Ca,Sr)TaO_2N series***

As previously described, compositions in this series were synthesised by first preparing the ternary $(Ca_pSr_{1-p})_2Ta_2O_7$ oxides for $0 < p < 1.0$ and then nitriding in flowing ammonia. Fig. 12 shows x-ray diffraction patterns of the oxide series, indicating a solid solution across the whole system.

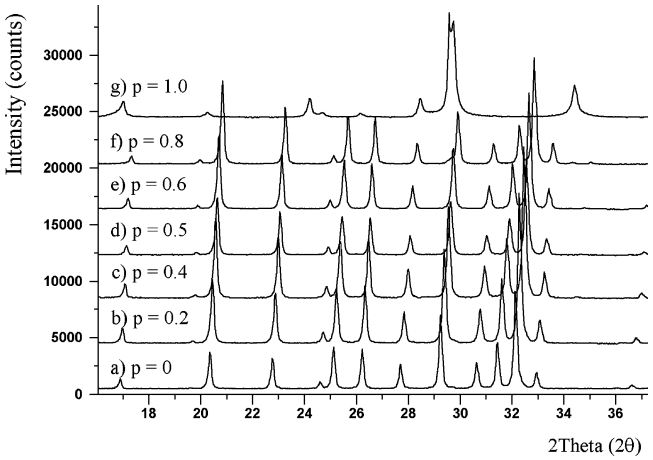

Fig. 12: X-ray diffraction patterns of pre-prepared $(Ca_pSr_{1-p})_2Ta_2O_7$ for $0 < p < 1.0$.

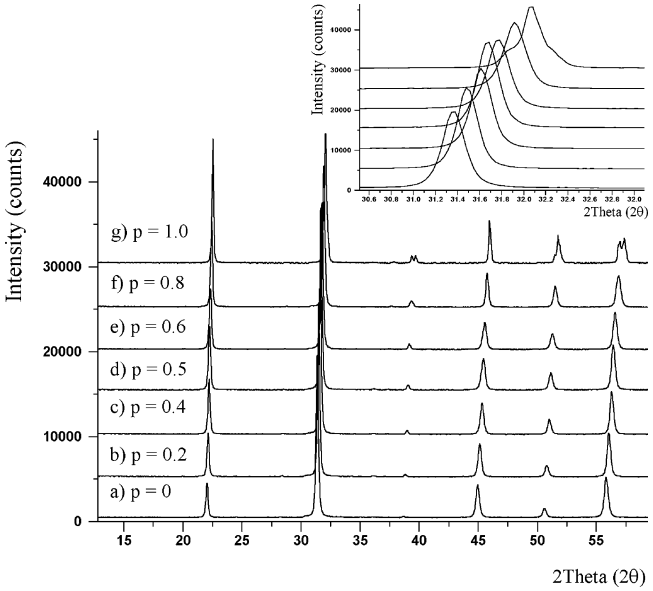

Fig. 13: X-ray diffraction patterns for $Ca_pSr_{1-p}TaO_2N$ for $0 < p < 1.0$.

After nitriding at 950 °C for 24 h followed by one regrinding and re-nitridation, essentially single-phase oxynitride products were obtained across the whole spectrum as indicated by the x-ray diffraction patterns in Fig. 13, which show a complete range of solid solution. The two end members in these solid solutions, $CaTaO_2N$ and $SrTaO_2N$, have been previously studied and determined as being orthorhombic and tetragonal, respectively [8]. In Ca-rich compositions, it was expected that the orthorhombic structure of $CaTaO_2N$ would predominate and the tetragonal type of structure at the Sr-rich end. Upon Ca substitution at $p > 0.6$, diffraction peaks tended to split into more peaks showing that the tetragonal Sr-rich structure was changing into the orthorhombic form for the more Ca-rich compositions (see Fig. 14). Unit cell dimensions, refined as tetragonal for $0 < p < 0.6$ and orthorhombic for $0.7 < p < 1.0$ are plotted out in Fig. 15. In the transition between tetragonal and orthorhombic, there is a uniform change from a_{tet} to a_o and from c_{tet} to b_o but there is a very clear change in gradient from a_{tet} to c_o.

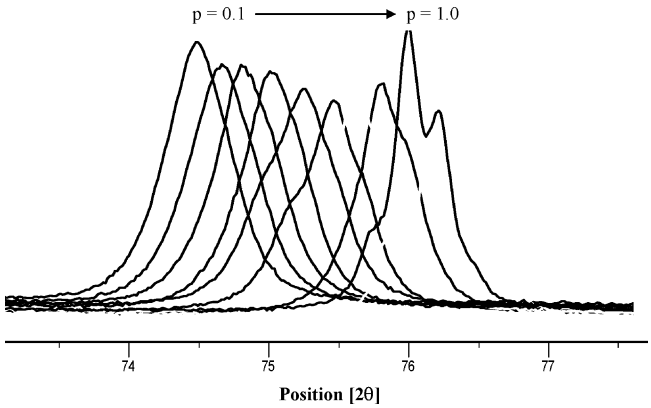

Fig. 14: X-ray diffraction patterns of the 75° 2θ peak showing an increasing tendency for orthorhombic distortion in Ca-rich $Ca_pSr_{1-p}TaO_2N$ compositions.

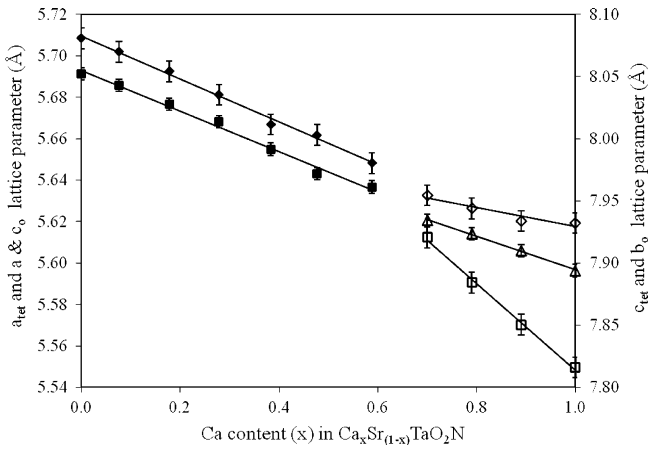

Fig. 15: Unit cell dimensions across the $Ca_pSr_{1-p}TaO_2N$ series, showing the tetragonal → orthorhombic transition at $0.6 < p < 0.7$.

Rietveld refinements were carried out for all compositions, using space group I4/mcm (as used by Günther *et al.* [8] for $SrTaO_2N$) for the tetragonal $0 < p < 0.6$ compositions and space group Pnma (used by Günther *et al.* [8] for $CaTaO_2N$) for orthorhombic $0.7 < p < 1.0$ compositions. All compositions refined well, giving final R-indices in the range of 2 – 4 %. Table 4 shows final parameters for tetragonal members of the series.

The only positional variable is the O/N(2) x parameter; the value for $SrTaO_2N$ (0.775) is in satisfactory agreement with the value of 0.772 obtained by Günther *et al.* [8], and with increasing calcium content, this parameter increases systematically, consistent with increasing rotation of octahedra away from their perfect perovskite positions. The comparison between the $p = 0$ ($SrTaO_2N$) and $p = 0.6$ compositions shown in Fig. 16 shows how little rotation occurs across the series. Table 5 shows final parameters for orthorhombic members of the series. The lower symmetry results in more positional variables; compared with the data provided by Günther *et al.* [8] for $CaTaO_2N$, refined x and z values for Ca and O/N(1) obtained in the present

work differ by approximately 0.004; a larger difference is observed for the O/N(2) x,y,z values. Looking at variations across the compositional range, the large cation position changes negligibly in z but the x-parameter steadily decreases with increasing strontium content. There are less clear shifts in the O/N positions, but overall, Fig. 17 shows that there is very little difference in the extent of rotation between p = 0.8 and p = 1.0 compositions. Refined site occupation factors always gave values close to their expected values.

Table 4: Final atomic coordinates for tetragonal I4/mcm $Ca_pSr_{1-p}TaO_2N$, $0 \le p \le 0.6$.

Atom	Wyckoff	Occupancy	x	y	z	R_p,R_{wp}
p = 0						2.4, 3.2
Sr	4b	1.000(7)	0	½	¼	
Ta	4c	1.0	½	½	0	
O/N(1)	4a	1.0	0	0	¼	
O/N(2)	8h	1.0	0.775(2)	0.275(2)	0	
p = 0.1						2.0, 3.0
Ca/Sr	4b	0.076(8)/0.924(8)	0	½	¼	
Ta	4c	1.0	½	½	0	
O/N(1)	4a	1.0	0	0	¼	
O/N(2)	8h	1.0	0.777(1)	0.277(1)	0	
p = 0.2						2.1, 3.1
Ca/Sr	4b	0.178(8)/0.822(8)	0	½	¼	
Ta	4c	1.0	½	½	0	
O/N(1)	4a	1.0	0	0	¼	
O/N(2)	8h	1.0	0.776(1)	0.276(1)	0	
p = 0.3						2.2, 3.3
Ca/Sr	4b	0.279(8)/0.721(8)	0	½	¼	
Ta	4c	1.0	½	½	0	
O/N(1)	4a	1.0	0	0	¼	
O/N(2)	8h	1.0	0.782(1)	0.282(1)	0	
p = 0.4						2.3, 3.5
Ca/Sr	4b	0.383(9)/0.617(9)	0	½	¼	
Ta	4c	1.0	½	½	0	
O/N(1)	4a	1.0	0	0	¼	
O/N(2)	8h	1.0	0.781(2)	0.281(2)	0	
p = 0.5						2.3, 3.6
Ca/Sr	4b	0.477(9)/0.523(9)	0	½	¼	
Ta	4c	1.0	½	½	0	
O/N(1)	4a	1.0	0	0	¼	
O/N(2)	8h	1.0	0.783(2)	0.283(2)	0	
p = 0.6						2.4, 3.8
Ca/Sr	4b	0.588(9)/0.412(9)	0	½	¼	
Ta	4c	1.0	½	½	0	
O/N(1)	4a	1.0	0	0	¼	
O/N(2)	8h	1.0	0.788(1)	0.288(1)	0	

Table 5: Refined atomic coordinates for orthorhombic Pnma $Ca_pSr_{1-p}TaO_2N$ compositions in the range $0.7 \leq p \leq 1.0$.

Atom	Wyckoff	Occupancy	x	y	z	R_p, R_{wp}
p = 0.7						1.8, 2.8
Ca/Sr	4c	0.70(3)/0.30(3)	0.989(1)	¼	0.998(5)	
Ta	4b	1.0	0	0	½	
O/N(1)	4c	0.67/0.33	0.462(4)	¼	0.062(6)	
O/N(2)	8d	0.67/0.33	0.275(3)	0.033(3)	0.708(3)	
p = 0.8						1.8, 2.8
Ca/Sr	4c	0.79(3)/0.21(3)	0.0190(7)	¼	0.998(3)	
Ta	4b	1.0	0	0	½	
O/N(1)	4c	0.67/0.33	0.466(3)	¼	0.077(3)	
O/N(2)	8d	0.67/0.33	0.280(2)	0.031(2)	0.709(2)	
p = 0.9						2.1, 3.3
Ca/Sr	4c	0.89(4)/0.11(4)	0.0288(6)	¼	0.995(2)	
Ta	4b	1.0	0	0	½	
O/N(1)	4c	0.67/0.33	0.485(3)	¼	0.076(2)	
O/N(2)	8d	0.67/0.33	0.282(2)	0.041(1)	0.713(2)	
p = 1.0						2.8, 4.5
Ca	4c	1.00(4)	0.0347(7)	¼	0.994(2)	
Ta	4b	1.0	0	0	½	
O/N(1)	4c	0.67/0.33	0.478(3)	¼	0.080(2)	
O/N(2)	8d	0.67/0.33	0.281(2)	0.046(1)	0.713(2)	

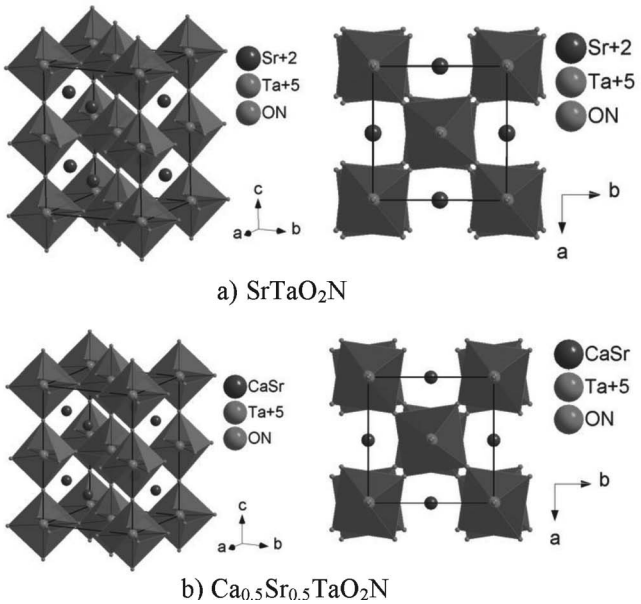

Fig. 16: [001] and [010] projections of (a) $SrTaO_2N$ and (b) $Ca_{0.5}Sr_{0.5}TaO_2N$ compositions in the tetragonal $Ca_pSr_{1-p}TaO_2N$ series.

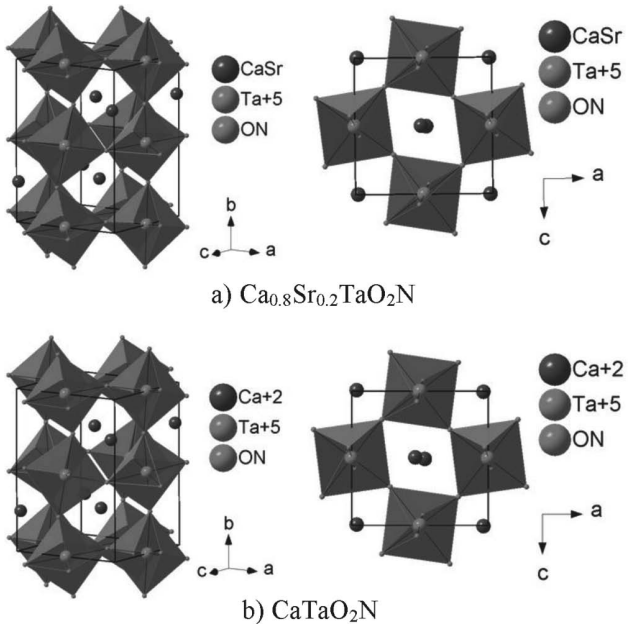

Fig. 17: [001] and [010] projections of (a) p = 0.8 and (b) p = 1.0 compositions in the orthorhombic $Ca_pSr_{1-p}TaO_2N$ series.

(c) ***The (Ba,Ca)TaO_2N series***

Attempts to produce members of this series were complicated by the absence of a $Ba_2Ta_2O_7$ intermediate compound. Direct ammonolysis of mixtures of $BaCO_3$, $CaCO_3$ and Ta_2O_5 was therefore explored in an attempt to produce (Ba,Ca)TaO_2N solid solutions, but in fact no products of this type were produced. Clearly, the disparity in size between the two large cations makes a perovskite phase less stable than mixes of other compounds.

IV. Discussion

The present work has focused on perovskite oxynitrides of the type $LnTiO_2N$, where Ln = La, Nd (and mixtures of these), and also $MTaO_2N$, where M is Ca, Sr, Ba (or mixtures), and in both series there are extensive ranges of solid solution. In the $MTaO_2N$ series, departures from perfect cubic symmetry are determined by the size of the M cation, with barium-rich compositions retaining the highest Pm3m symmetry and strontium-rich compositions lowering the symmetry to tetragonal (I4/mcm). Calcium-rich compositions showed orthorhombic symmetry, always in space group Pnma. For the $LnTiO_2N$ series, lanthanum-rich compositions refined satisfactorily in space group Imma consistent with the work of Yashima *et al.* [9], whereas $NdTiO_2N$ and most compounds in the solid solution series between the Nd and La end-members refined more satisfactorily in space group Pnma, consistent with the work of Clarke *et al.* [6]. The current study did not explore the possibility of solid solution between $LnTiO_2N$and $MTaO_2N$ oxynitrides, but the present results suggest that this would be a strong possibility. A series of more nitrogen-rich oxynitrides, having compositions of the type $LnTaON_2$ [10], with perovskite structures exhibited by the larger rare earths (Ln = La – Sm) and pyrochlore structures by the higher atomic number members offer possibilities for further study of perovskite solid solution in these oxynitride systems.

The Rietveld crystal structure refinements for compositions in the $LnTiO_2N$ series showed few surprises. For the $MTaO_2N$ series, in cubic (Ba-rich) oxynitrides, octahedra were precisely aligned with the unit cell edges, and with symmetry degeneration to tetragonal and then to orthorhombic, the Ta-centred octahedra rotated further away from the perfect cubic positions with associated symmetry degeneration. The assumption of random occupation of the large cation site in all solid solution series seemed fully justified; the assumption of random occupation of the non-metal sites by oxygen and nitrogen could not be tested in the present study, and further work by neutron diffraction would be required to detect any ordering behaviour.

V. Conclusions

Perovskite-type oxynitrides of the type ABO_2N do not permit as wide a range of cation substitutions as in the pure oxide counterparts, but nevertheless display similar structural features. The compounds which have received most attention are those with the B cation being either Ti^{4+} or Ta^{5+}, with rare earths as the A cation in the first series, and Group II metals as the A cation in the second.

In the $LnTiO_2N$ series, lanthanum appears to be unique in not displaying the Pnma symmetry found for $NdTiO_2N$ (and probably higher Ln atomic number $LnTiO_2N$ compounds as well). In mixed (La,Nd)TiO_2N perovskites, the transition from Pnma to Imma occurs at slightly more La-rich compositions than a La : Nd ratio of ~ 0.8.

In $MTaO_2N$ oxynitrides, with M = Ca, Sr or Ba, there is virtually no range of solid solution between Ca and Ba end-members because of the large disparity in cation sizes. However, the Ba,Sr series exhibit complete solid solution, changing from the cubic Pm3m $BaTaO_2N$ to the tetragonal I4/mcm $SrTaO_2N$ at approximately p = 0.5 – 0.6 in the general formula $Ba_pSr_{1-p}TaO_2N$, consistent with the results of Pors *et al.* [7]. The Ca,Sr series also show a complete range of solid solution varying between the tetragonal I4/mcm $SrTaO_2N$ to the orthorhombic Pnma $CaTaO_2N$; again, the change in structure is not easy to determine accurately by Rietveld refinement using x-ray powder data, but is approximately at the composition p = 0.6 – 0.7 in the general formula $Ca_pSr_{1-p}TaO_2N$. A more accurate determination of these figures could be obtained by a future study using neutron diffraction data.

References

1 Thompson, D.P.: Oxynitride research in the nano era, *Mater. Sci. Forum,* **554**, 1 – 10, (2007).

2 Marchand, R., Pors, F., Laurent, Y.: Preparation and characterization of new oxynitrides with a perovskite structure, (in French), *Rev. Int. Hautes Tempér. Réfract. Fr*., **23**, 11 – 15, (1986).

3 Gouin, X., Marchand, R., Laurent, Y., Gervais, F.: Infrared dielectric response of $BaTaO_2N$, *Sol. State Comms.,* **93**, 857 – 9, (1995).

4 Kim, Y.-I., Woodward, P.M., Baba-Kishi, K.Z., Tai, C.W.: Characterization of the structural, optical and dielectric properties of oxynitride perovskites AMO_2N (A = Ba, Sr, Ca; M=Ta,Nb), *Chem. Mater.,* **16**, 1267 – 76, (2004).

5 Marchand, R., Laurent, Y., Guyader, J., L'Haridon, P., Verdier, P.: Nitrides and oxynitrides: preparation, crystal chemistry and properties, *J. Eur. Ceram. Soc*., **8**, 197 – 213, (1991).

6 Clarke, S.J., Guinot, B.P., Michie, C.W., Calmont, M.J.C., Rosseinsky, M.J.: Oxynitride perovskites: synthesis and structures of $LaZrO_2N$, $NdTiO_2N$ and $LaTiO_2N$ and comparison with oxide perovskites, *Chem. Mater.,* **14**, 288 – 94, (2002).

7 Pors, F., Bacher, P., Marchand, R., Laurent, Y., Roult, G.: Structural study of the oxynitride perovskite $SrTaO_2N$ and the solid solution $Ba_{1-x}Sr_xTaO_2N$ by neutron diffusion, *Rev. Int. Hautes Tempér. Réfract. Fr*., **24**, 239 – 46, (1988).

8 Günther, E., Hagenmayer, R., Jansen, M.: Structural studies of the oxynitrides $SrTaO_2N$, $CaTaO_2N$ and $LaTaON_2$ by means of neutron and X-ray diffraction, (in German), *Z. Anorg. Allg. Chem*., **626**, 1519 – 25, (2000).

9 Yashima, M., Saito, M., Nakano, H., Takata, T., Ogisu, K., Domen, K.: Imma perovskite-type oxynitride $LaTiO_2N$: structure and electron density, *Chem. Comm*., **46**, 4704 – 6, (2010).

10 Jansen, M., Letschert, H.P.: Inorganic yellow-red pigments without toxic metals, *Nature*, **404**, 980 – 82, (2000).